Spectroscopic determination of the water dimer intermolecular potential-energy surface

N. Goldman
Department of Chemistry, University of California, Berkeley, California 94720

R. S. Fellers
Yahoo!, Santa Clara, California 95051

M. G. Brown
Department of Chemistry, University of Oregon, Eugene, Oregon 97403

L. B. Braly
Lam Research Corp., Fremont, California 94538

C. J. Keoshian
Department of Chemistry, University of California, Berkeley, California 94720

C. Leforestier
LSDSMS (UMR 5636)-CC 014, Université Montpellier II, 34095 Montpellier Cedex, France

R. J. Saykally[a)]
Department of Chemistry, University of California, Berkeley, California 94720

(Received 12 December 2001; accepted 19 March 2002)

Two polarizable six-dimensional water dimer intermolecular potential surfaces have been determined by fitting the distributed multipole ASP (anisotropic site potential) potential form to microwave, terahertz, and midinfrared cavity ringdown $(D_2O)_2$ spectra via a rigorous calculation of the water dimer eigenstates with the PSSH (pseudo-spectral split Hamiltonian) method. The fitted potentials accurately reproduce most ground-state vibration-rotation-tunneling spectra and yield excellent second virial coefficients for both H_2O and D_2O. The calculated dimer structure and dipole moment are close to those determined from microwave spectroscopy and high level *ab initio* calculations, except that the O–O distance (2.952 Å) is significantly shorter than the currently accepted experimental value. The dimer binding energy (4.85 kcal/mol) is considerably smaller than the accepted experimental result, but in excellent agreement with recent theoretical results, as are the acceptor switching and donor–acceptor interchange tunneling barriers and the cyclic water trimer and tetramer structures and binding energies. © *2002 American Institute of Physics.*
[DOI: 10.1063/1.1476932]

I. INTRODUCTION

The quest to accurately describe the solid and liquid phases of water has precipitated the development of an enormous number of effective intermolecular potential surfaces (IPS) for use in computer simulations.[1] Such effective potentials are widely and effectively used in many areas of science but their limitations are well known, and include a restricted accuracy and instability when used outside of the parameterized temperature and pressure range. These limitations arise primarily from the unphysical description of the crucial many-body interactions among water molecules in the potential, which are usually expressed only implicitly through the fitted values of the parameters, although some IPS include polarizability–the leading many-body term.

Two approaches have been pursued to improve this situation. *Ab initio* molecular dynamics[2] ostensibly transcends the difficulties in representing the force field, although the dispersion interactions are not properly accounted for in the density functional theory underlying the method, whereas dispersion is known to constitute ca. 20% of the cohesive energy of liquid water.[3] Moreover, computational limitations restrict these treatments to small ensembles (e.g., 32 or 64 molecules).[4,5] Another approach is to properly separate the pairwise, three-body, four-body, etc. interactions, while still keeping a relatively simple potential form that is usable in large scale simulations. This can, in principle, be accomplished through the detailed spectroscopic investigation of small water clusters, as the *n*-body interactions in water have been shown to converge rapidly. In particular, the water dimer provides a direct route to the pair potential, the trimer to the three-body interactions, and so on.

This partitioning of the *n*-body interactions can be accomplished via *ab initio* calculations,[6] however, exchange-repulsion and dispersion forces are notoriously difficult to calculate with sufficient accuracy. Since these terms constitute a large fraction of the total interaction energy, and since they also strongly influence the detailed topology of the IPS (e.g., hydrogen bond rearrangement pathways), it is advanta-

a)Author to whom correspondence should be addressed. Electronic mail: saykally@uclink4.berkeley.edu

geous, if not essential, to parameterize (or ''tune'') a potential against high resolution spectroscopic data.

Inversion of experimental data to produce a quantitatively accurate intermolecular potential surfaces is not a new idea, although computational limitations have restricted previous efforts to weakly bound systems of low dimensionality such as (1) rare gas (Rg) pairs[7] (one intermolecular degree of freedom), (2) Rg–H_2[8] and Rg-hydrogen halides[9–12] (two intermolecular degrees of freedom), (3) Ar–H_2O[13,14] and Ar–NH_3[15] (three intermolecular degrees of freedom), and (4) $(HCl)_2$[16] (four intermolecular degrees of freedom). The largest difficulty in attempting to invert spectroscopic data for larger systems is that the CPU time generally scales as $(O(1000^D)$, where D is the number of degrees of freedom. Despite such limitations, Olthof, van der Avoird, and Wormer accomplished an impressive determination of the six-dimensional $(NH_3)_2/(ND_3)_2$ pair potential by a trial-and-error variation of some of the exchange-repulsion terms to force agreement with vibration-rotation-tunneling (VRT) data. The magnitude of the calculation precluded determination of the potential by direct regression analysis, however, the resulting ''tuned'' potential reproduces the measured spectroscopic properties of the ammonia dimer very well,[17] and reconciles a long standing debate between theory and experiment regarding the nature of hydrogen bonding in this important paradigm.

With the wealth of water dimer VRT data that have been compiled by our group,[18,19] coupled with recent advances in computational methods,[20–22] it is now possible to accurately calculate the VRT states of a six-dimensional system within a nonlinear least-squares fitting approach. In a recent publication, we described the determination of a water pair potential by direct regression analysis of the rotational constants, tunneling splittings, and intermolecular vibrational frequencies precisely determined from microwave and terahertz VRT spectroscopy of the water dimer.[23] The 6D (frozen monomer) IPS that resulted from this fit, VRT(ASP-W), represented a qualitative improvement in the analytical description of the water dimer potential, and VRT(ASP-W) was also found to model the ground-state properties of the water trimer and tetramer quite well. Shortly after the publication of the VRT(ASP-W) potential determination, Groenenboom *et al.*[24,25] reported their determination of a 6D (frozen monomer) water dimer IPS, effected by ''tuning'' the high quality *ab initio* surface of Mas *et al.*[26,27] to achieve agreement with the $(H_2O)_2$ VRT data. Their IPS is of comparable accuracy to that of VRT(ASP-W), and actually describes some properties better.

Due to limited computing resources, our VRT(ASP-W) fit was made tractable by truncating the induction terms to first-order. For the description of the dimer, this results in a small error in the IPS description. However, due to the many-body nature of the induction term, this error is compounded in larger clusters. Improvements in both the fitting code and computational resources now permit us to refit the dimer potential with converged self-consistent induction on a reasonable time scale. Six new terahertz transitions have also been included in this improved fit using the ASP-W potential.[18] The ASP-W was chosen over the newer ASP-W2 and ASP-W4 since it produces perfect agreement with the second viral coefficient and behaves quite similarly to the two newer versions. Additionally, these parameterizations were not available in Fortran, which presented computational problems. The present paper describes the determination and thorough testing of an improved water dimer potential, VRT(ASP-W)II. A second fit was subsequently performed using some data that was excluded from the VRT(ASP-W)II fit (Acceptor Wag transitions),[18] as well as two new donor torsions transitions that were measured since the VRT(ASP-W)II fit was performed. This newest dimer potential-energy surface, called VRT(ASP-W)III, constitutes a slight refinement over its predecessors. We present both new IPS here because version II was tested much more thoroughly against larger clusters and second virial coefficient data, all of which was highly computationally demanding and thus did not permit us to repeat the calculations for the refined IPS.

II. METHODS

A. Theoretical aspects

In previous publications[20–22] we discussed the method of calculating the VRT states of the water dimer in a six-dimensional fully coupled dynamical formalism. For completeness we briefly summarize the method. The Hamiltonian expressed in scattering coordinates is

$$H = -\frac{\hbar^2}{2\mu_{AB}}\frac{\partial^2}{\partial R^2} + H_{\mathrm{rot}}^{(A)} + H_{\mathrm{rot}}^{(B)} + V(R,\Omega^{(A)},\Omega^{(B)}) + \frac{1}{2\mu_{AB}R^2}\{\mathbf{J}^2 + \mathbf{j}^2 - 2\mathbf{j}\cdot\mathbf{J}\}.$$

Here μ is the cluster reduced mass, H_{rot} are the monomer Hamiltonians, V is the potential in terms of center-of-mass separation (R), and Euler angles (Ω), $\mathbf{J}$ is the cluster angular momentum, and $\mathbf{j}$ is the sum of the monomer angular momenta $(\mathbf{j}_A+\mathbf{j}_B)$. The basis comprises Wigner functions describing the monomer and cluster angular components and sine functions for the radial component. To evaluate the action of the Hamiltonian, we use the PSSH method, wherein the kinetic-energy terms are evaluated analytically and the potential energy is determined by means of Gaussian quadratures on a six-dimensional grid. This method allows us to avoid dealing explicitly with the Hamiltonian matrix $(O(N^6))$. The lowest eigenvalues/eigenvectors of interest are obtained iteratively by a Lanczos recursion scheme.

The size of the basis is defined by the range of the allowed monomer quantum numbers and the number of radial sine functions. A monomer basis of $j_{\max}=k_{\max}=\omega_{\max}=10$ and a radial basis of ten elementary sine functions is sufficient to converge the absolute energies to <0.2 cm^{-1} and the relative energies to <0.02 cm^{-1} in the ground state. For the remaining discussion, we will assume that $j_{\max}=k_{\max}=\omega_{\max}$ is always true and will refer to the basis size by quoting the $j_{\max}$ value.

B. Experimental data

Since the first high resolution microwave study of $(H_2O)_2$ in 1977 by Dyke and Muenter[28] there have been a

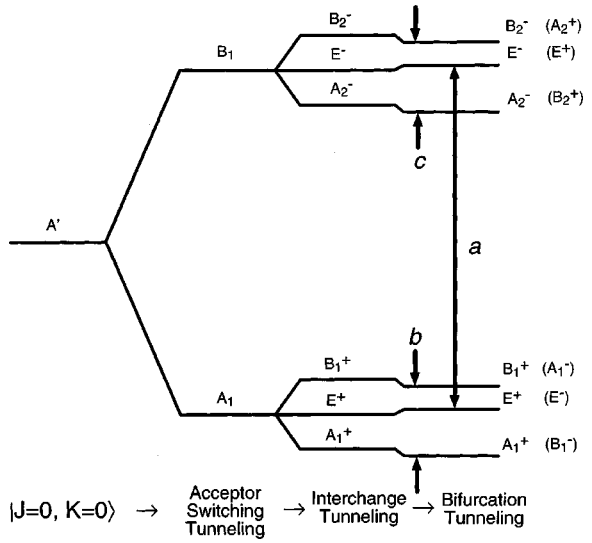

FIG. 1. The effect of the three tunneling motions on lowest-energy water dimer rovibrational state with labeled splittings. The symmetry labeling scheme is determined from Permutation Inversion group theory (Ref. 29). These labels describe the symmetry of the different water dimer tunneling wave functions. The splitting or shift of the VRT states is inversely related to the tunneling barriers. Acceptor Switching, which has the smallest barrier, causes each rovibrational state to be split into two: A_1 and B_1. Interchange tunneling further splits each of those states into three. Bifurcation tunneling, which has the highest barrier, causes a small shift of the $E^{-/+}$ states but does not cause further splitting because the first two motions have already resolved all the available states. The unbracketed labels apply to the $J=0$ state of the ground state or symmetric (A') vibrational modes. The labels in parentheses apply to the $J=0$ states of antisymmetric (A'') vibrational modes. For $K\neq 0$ states, K-type asymmetry doubling causes each state to be split again (on the order of unit MHz) so that all ten symmetries are permitted for each J level. Each of the three sets of states (e.g., $A_1^+/E^+/B_1^+$ and $A_2^-/E^-/B_2^-$) produced by interchange tunneling is called an "interchange triplet." Interchange triplets are conveniently referenced by the numeral subscript of the constituent states. For example, the $A_1^+/E^+/B_1^+$ interchange triplet is also labeled as "1."

number of published reports on radio frequency, microwave, terahertz (far-IR), and mid-IR spectra of $(H_2O)_2$, $(D_2O)_2$, and mixed isotope water dimers which provide an accurate characterization of the ground state for the various isotopomers of this cluster.[29–39] At present, there exist hundreds of precisely measured transitions in the microwave and far-IR, as described in Papers I[18] and II.[19] Because there are three distinct rearrangement pathways that can exchange the positions of the hydrogens within the dimer without breaking covalent bonds, each rovibrational state of the homodimers is split into six distinct VRT states if $|K|=0$, or ten distinct VRT states if $|K|>0$ (see Ref. 18). Schematics of the ordering of the VRT states for $J=0$ in the ground state are presented in Fig. 1. The dimer equilibrium structure determined in this work is shown in Fig. 2.

For $(D_2O)_2$, the ground-state interchange and bifurcation tunneling splittings have been characterized to 1×10^{-6} (ca. 1 MHz) accuracy in microwave experiments[31,32,35] and the acceptor switching tunneling splitting is known to within 1 GHz.[39] Less detailed information is available for $(H_2O)_2$ due to a lack of experimental data as a result of unfavorable spin statistics.

At the time that the work described in this paper was

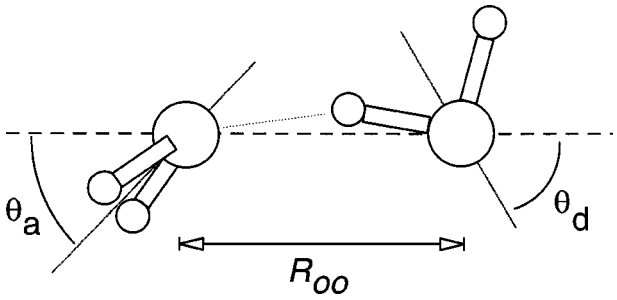

FIG. 2. The water dimer equilibrium structure determined in this work.

commenced, we had accumulated spectra describing fundamental intermolecular vibrations of $(D_2O)_2$ at 65, 83, 90, and 104 cm^{-1}.[18,36,37] Within the 83 cm^{-1} band, both $|K|=0,1$ manifolds have been completely measured. The 83 cm^{-1} band has A' vibrational symmetry and is believed to be the ν_8 acceptor bend. Characterization of the 65 cm^{-1}, A'', ν_{12} donor torsion is also now complete. New data from the 65 cm^{-1} and 90 cm^{-1} bands were included in the present fit that were not in the original VRT(ASP-W)II fit.

Our understanding of $(H_2O)_2$ is much less complete. We have observed bands at 87, 102, 103, 108, 120, and 140 cm^{-1}.[19] Unfortunately, all the $(H_2O)_2$ bands are heavily perturbed (presumably due to strong Coriolis coupling[30]), which has hindered efforts to properly characterize these far-IR bands.

Because of the more limited $(H_2O)_2$ data, we decided to concentrate exclusively on determining a $(D_2O)_2$ potential via a nonlinear least-squares fit of the available spectroscopic data. A secondary goal of this work is to "bootstrap" the measurement and assignment of both $(D_2O)_2$ and $(H_2O)_2$ VRT data so that we eventually have a complete set of all allowed and precisely measured transitions for all isotopomers of the water dimer.

C. Form of the potential surface

We have investigated a number of water potential forms, including SPC,[40] polarizable SPC,[41] TIP4P,[42] ST2,[43] MCY,[44] MCY-KW,[45] SW,[46] NEMO,[47] ASP-S,[48] and ASP-W,[48] and have found ASP-W to best reproduce the VRT data and second virial coefficients in 6D frozen monomer calculations. In ASP-W, the interaction energy between water molecules is expressed as the sum of electrostatic, short-range repulsion, induction, and dispersion terms. The potential is parameterized using the perturbation theory (IMPT) of Hayes and Stone.[49] This scheme accounts for the overlap of the monomer wave functions and the Pauli antisymmetry principle from the outset. At long range, the electrostatic interaction is

$$E_{\rm es}=\sum_{a\in A}\sum_{b\in B}Q_t^a T_{tu}^{ab} Q_u^b,$$

where t and u label the multipoles and T_{tu}^{ab} is an interaction function, depending on the distance and relative orientation of the molecules. The Q_t^a and Q_u^b terms are spherical multipoles distributed on oxygen and hydrogen atoms fitted to the electronic density calculated at the MP2 level. The multipoles are truncated to quadrupole on the oxygens and di-

pole on the hydrogens. The electrostatic energy at short range, where wave function overlap causes the multipole expansion to break down, is accounted for by the penetration energy

$$E_{\mathrm{pen}}=E(\mathrm{IMPT})-E_{\mathrm{es}},$$

where E_{es} is the electrostatic energy in the long range formalism and $E(\mathrm{IMPT})$ is the total electrostatic energy, which includes the long-range contribution and short-range corrections. E_{pen} is absorbed in the exchange repulsion term.

Exchange repulsion is fitted to the functional form

$$E_{\mathrm{er}}=\sum_{a\in A}\sum_{b\in B} e^{-\alpha_{ab}(R_{ab}-\rho_{ab}(\Omega))},$$

with R_{ab} the distance between site a of molecule A and site b of molecule B, α_{ab} a hardness parameter depending on the site pair, and $\rho_{ab}(\Omega)$ an orientation-dependent parameter describing the effective size of the atoms. The expanded form of ρ for a single site is

$$\rho_a(\theta,\phi)=\sum_{lk}\rho_{lk}^{a}C_{lk}(\theta,\phi),$$

where C_{lk} are renormalized spherical harmonics and with the site-site interaction term formed as

$$\rho_{ab}(\Omega)=\rho_a(\Omega)+\rho_b(\Omega).$$

The induction energy is also determined by IMPT and parameterized as single site oxygen centered polarization tensor with a multipole expansion up to octopole. At short range, overlap effects are modeled by Tang–Toennies damping functions $f_n(R)$:

$$f_n(R)=1-e^{-aR}\sum_{k=0}^{n}\frac{(aR)^k}{k!}.$$

The induction energy is found by

$$E_{\mathrm{ind}}=\frac{1}{2}\sum_{A}\sum_{B\neq A}\Delta Q_t^a T_{tu}^{ab} f_n(R_{ab})^{1/2} Q_u^b,$$

and

$$\Delta Q_{t'}^{a'}=-\sum_{B\neq A}\alpha_{t't}^{a'a}T_{tu}^{ab}f_{n'}(R_{a'b})^{1/2}(Q_u^b+\Delta Q_u^b),$$

where Q_t^a are permanent multipoles of molecule A, ΔQ_t^a induced multipoles of molecule A, $\alpha_{t't}^{a'a}$ the polarizability tensor, R_{ab} the distance between the sites concerned, and the index n or n' of the damping function equal to $2l_1+2l_2+2$ for the interaction between multipoles of rank l_1 and l_2. With the inclusion of ΔQ_u^b, we are making the assumption that the induction energy is determined iteratively. In Millot and Stone's original formulation, induction is not iterated to self-consistency but is instead computed by a single pass through the induction routine to reduce the execution time. Millot and Stone find that with a single pass, the induction energy is within 10% of the fully converged value.[48] In our earlier determination of the VRT(ASP-W) surface,[23] we employed their first-order approach, but for the present calculations we iterate the induction energy to full convergence. The polarizability tensor is determined at the SCF level and scaled so that α_{xx}, α_{yy}, and α_{zz} replicate the experimental values of 10.311, 9.549, and 9.907 a.u., respectively.

Millot and Stone[48] explain that the IMPT method is not very accurate at determining the dispersion energy and for this reason they employ the dispersion coefficients of Rijks and Wormer.[50] These values are calculated using the Casimir–Polder integral[51] with frequency dependent polarizabilities derived by a double perturbation technique that accounts for intermolecular and intramolecular correlations. Dispersion terms C_6 through C_{10} are fitted to a single center multipole expansion on the water monomer center-of-mass. The dispersion energy is found in ASP as

$$E_{\mathrm{disp}}=-\sum_{n=6}^{10}\sum_{l_Ak_Al_Bk_BL}\frac{C_n^{l_Ak_Al_Bk_BL}}{R^n}\times A_{l_Ak_Al_Bk_BL}(\omega_A,\omega_B,\omega)f_n(R),$$

where R is the distance between the centers-of-mass, $C_n^{l_Ak_Al_Bk_BL}$ is a dispersion coefficient, $A_{l_Ak_Al_Bk_B}(\omega_a,\omega_b,\omega)$ a function of the orientation ω_a and ω_b of the two molecules in space and ω specifying the orientation of the intermolecular vector, and $f_n(R)$ a Tang–Toennies damping function. Throughout this work, the monomer geometry is fixed at the equilibrium structure of $<\mathrm{HOH}=104.52°$ and $R_{\mathrm{OH}}=0.9572$ Angstroms. This neglects the slight elongation of the donor O–H bond lengths and the slight distortion of the H–O–H bond angle that accompanies hydrogen-bond formation.

D. Least-squares fit

The fully coupled six-dimensional PSSH calculation was embedded in a standard nonlinear least-squares fitting routine (Levenberg–Marquardt algorithm).[52] The matrix of derivatives is determined via the Hellman–Feynman theorem

$$\frac{\partial E}{\partial p_i}=\left\langle \Psi\left|\frac{\partial V}{\partial p_i}\right|\Psi\right\rangle,$$

where p_i is the ith parameter of potential V and Ψ is an eigenvector. One-sided numerical derivatives are used to determine the elements of the $\delta V/\delta p_i$ grid. The eigenvectors are also used as Lanczos seed vectors for the subsequent calls to the energy routine. If the potential is only slightly perturbed between fitting iterations, using the eigenvectors saved from the previous iteration as seed vectors can reduce the required number of Lanczos iterations by as much as 50%. For the angular basis we used functions up to $j_{\max}=10$ and for the radial basis we used a range of 4.00–8.00 au. We contracted ten elementary sine functions using the HEG scheme[22] and retained six contracted functions for the energy calculation. With this basis, we can converge the lowest $J=0,1$ eigenstate of a single symmetry to within $\pm 10^{-5}$ cm^{-1} in approximately 1 hour on a 733 MHz Pentium III computer. The total time to calculate the energies of all the $J=0$ and $J=1$ symmetries up to 150 cm^{-1} above the lowest eigenstate is then on the order of 12 hours.

As previously noted, the number of observed $(D_2O)_2$ microwave and terahertz transitions number is very large. Certainly, one would like to use as much experimental data

TABLE I. Nonzero real components of the atomic multipole moments of the water molecule (spherical tensors in atomic units) at the MP2 level.

	Oxygen		
Q_{00}	−0.675 363		
Q_{10}	0.095 022		
Q_{20}	−0.061 205	Q_{22c}	0.644 597
	Hydrogen		
Q_{00}	0.337 681		
Q_{10}	−0.072 850 82	Q_{11c}	0.002 487 997 9

as possible to rigorously constrain the water dimer IPS. However, a number of factors preclude the use of these complete data, including:

1) Memory constraints limit our fit to $J=K\leqslant 1$.

2) Most of the observed transitions are highly correlated, that is, only a small subset provide unique information with respect to the shape of the water dimer IPS.

3) The positions of the E states with respect to the A/B states in a given interchange triplet characterize the bifurcation tunneling. These shifts of the E states, however, are very small, ca. 5 MHz in the ground state. This is smaller than the convergence properties of our calculation and so these states are unable to provide useful constraints on the ground-state bifurcation tunneling.

4) In order to use experimentally determined tunneling-splitting data characteristic of a given vibrational band, the calculated eigenstates must be assigned to distinct vibrational modes. Presently, we do not have a reliable method to automatically make the vibrational assignments. Fortunately, symmetry restrictions on the $K_a=0$ states allow us to assign individual $K_a=0$ states to either A' or A'' vibrational symmetry. For example, in an A' mode, the allowed symmetries for $J=K_a=0$ are $A_1^+/E^+/B_1^+/A_2^-/E^-/B_2^-$. Since there are no symmetry restrictions on the $K_a\geqslant 1$ states, i.e., all possible $A/E/B$ symmetries are observed regardless of the vibrational symmetry, assignment of individual states to specific vibrational bands becomes difficult. If two or more bands are nearly degenerate, it becomes impossible to assign these states to a unique vibrational mode. As the reader will see, there are three nearly degenerate bands clustered around 80 cm^{-1} in the $(D_2O)_2$ spectra that currently prevent us from using the excited state manifold in the fit.

With these considerations in mind, we find that we can capture the most salient features of the water dimer IPS by calculating the following symmetries for $J=0$ and $J=1$:

$$J=0 \quad A_1^+/B_1^+/A_1^-/B_1^-/A_2^+/B_2^+/A_2^-/B_2^-$$

$$J=1 \quad A_1^-/B_1^-/A_2^+/B_2^+/A_2^-/B_2^- .$$

Using this reduced set of eigenstates reduces the computing time and memory requirements considerably. The data used in the fit consist of 30 microwave and far-IR transitions as well as tunneling splittings precisely derived from spectra (Table VII).

The ASP-W potential form is quite sophisticated and attempts to describe the four contributions to the intermolecular forces (i.e., electrostatic, exchange-repulsion, dispersion, and induction) with unprecedented accuracy. The potential consists of 72 parameters, not counting the terms that describe the (frozen) monomer geometry. If we remove the electrostatic terms (determined at the MP2 level of theory) and the induction terms (scaled to experimental data) as constants, there are still 50+ parameters describing dispersion, exchange-repulsion, and damping terms in the model.

Due to computational limitations, it is not feasible to fit all of the remaining parameters so we must be judicious in our selection. In our previous IPS determinations, we found that the spectroscopic properties are most sensitive to the details of the exchange-repulsion.[23] In the original effort, we fit VRT(ASP-W) by adjusting a total of eight exchange-repulsion parameters and produced a surface that satisfactorily described most observed VRT spectra, second virial coefficients, and water dimer, trimer, and tetramer ground-state structures. As mentioned previously, the potential fit required two important approximations to reduce computational time: truncating the number of retained HEG DVR points that de-

TABLE II. Parameters for the exchange-repulsion-penetration energy: α ($bohr^{-1}$), ρ_0 and ρ_{lk} (bohr).

			Oxygen–Oxygen				
α^{OO}	2.002 732	p_0^{OO}	5.639 166				
			Oxygen–Hydrogen				
α^{OH}	1.980 393	p_0^{OO}	4.723 144				
			Hydrogen–Hydrogen				
α^{HH}	1.929 894	p_0^{HH}	3.824 493				
			Oxygen anisotropy				
ρ^{O}_{10}	0.194 693						
ρ^{O}_{20}	−0.395 620	ρ^{O}_{22c}	0.099 227				
ρ^{O}_{30}	0.360 409	ρ^{O}_{32c}	−0.204 826				
ρ^{O}_{40}	−0.117 409	ρ^{O}_{42c}	0.070 905				
			Hydrogen anisotropy				
ρ^{H}_{10}	−0.402 480	ρ^{H}_{11c}	−0.281 719				
ρ^{H}_{20}	0.006 327	ρ^{H}_{21c}	−0.143 812	ρ^{H}_{22c}	0.032 326		
ρ^{H}_{30}	0.068 294	ρ^{H}_{31c}	0.074 584	ρ^{H}_{32c}	0.026 826	ρ^{H}_{33c}	0.142 389

TABLE III. Parameters $C_n(l_1,l_2,j,\kappa_1,\kappa_2)$ (mHartree bohr^n) for the dispersion energy of the water dimer.

n	l_1	l_2	j	κ_1	κ_2	$C_n(l_1,l_2,j,\kappa_1,\kappa_2)$
6	0	0	0	0	0	487 93.883
6	2	0	2	2c	0	2009.963
6	2	2	4	2c	2c	265.308
6	2	0	2	0	0	140.963
7	1	0	1	0	0	−981 57.112
7	3	0	3	2c	0	−215 53.319
7	3	0	3	0	0	114 03.674
8	0	0	0	0	0	1 227 482.6
8	1	1	2	0	0	177 141.8
8	2	0	2	2c	0	83 283.1
8	2	0	2	0	0	76 265.5
8	4	0	4	2c	0	64 190.5
8	1	1	0	0	0	−55 356.8
8	3	3	6	2c	2c	48 697.6
8	4	0	4	0	0	−47 004.7
8	3	1	4	2c	0	42 175.4
9	1	0	1	0	0	−3 092 989.3
9	3	0	3	2c	0	−1 636 942.3
9	3	0	3	0	0	827 472.5
10	0	0	0	0	0	32 357 365
10	1	1	2	0	0	6 506 211
10	4	0	4	2c	0	4 842 514
10	4	0	4	0	0	−3 702 016
10	3	1	4	2c	0	3 699 920
10	2	0	2	0	0	2 491 946
10	1	1	0	0	0	−2 277 173
10	2	0	2	2c	0	1 995 054
10	3	3	6	2c	2c	1 888 239
10	3	1	4	0	0	−1 871 071

scribe the radial degree of freedom and truncating the iterated induction of VRT(ASP-W) to just one iteration. Even with these approximations, the total fitting time on three IBM RS6000/590's was about six months.

With recent performance improvements in the fitting code, we have been able to refit the potential with twice as many HEG points and with converged iterated induction to produce a more complete description of the water dimer IPS, VRT(ASP-W)II. Additionally, we reduced the number of fitted parameters, which govern the exchange-repulsion forces, from eight to four. Subsequently, further improvements were made on ASP-W by including five additional VRT transitions (corresponding to the acceptor wag and donor torsion) and fitting six exchange-repulsion parameters, which has resulted in a third IPS, VRT(ASP-W)III. DQMC calculations to determine D_e, average orientations of the dimer, and other properties were only performed on VRT(ASP-W)II. Hence, both it and VRT(ASP-W)III are presented in this paper, and VRT(ASP-W)III is presented as a refined version of VRT(ASP-W)II.

TABLE IV. Single-site polarizabilities of the water molecule up to rank 2 in real spherical tensor notation (atomic units). $\alpha_{l2\kappa2,l1\kappa1}$ is equal to $\alpha_{l1\kappa1,l2\kappa2}$. The origin of the sites is the oxygen atoms.

l_1	κ_1	l_2	κ_2	$\alpha_{l1\kappa1l2\kappa2}$	l_1	κ_1	l_2	κ_2	$\alpha_{l1\kappa1l2\kappa2}$
1	0	1	0	9.907	2	0	2	0	29.871
1	0	2	0	−4.249	2	0	2	2c	−0.425
1	0	2	2c	−4.409	2	1c	2	1c	52.566
1	1c	1	1c	10.311	2	1s	2	1s	28.179
1	1c	2	1c	−11.920	2	2c	2	2c	37.273
1	1s	1	1s	9.549	2	2s	2	2s	31.449
1	1s	2	1s	−3.575					

TABLE V. The fitted exchange-repulsion-penetration constants of VRT(ASP-W)II (a) and III (b). Uncertainties are listed in parentheses. The original (unfitted) values are listed in Table II.

(a) VRT(ASP-W)II	
ρ^{O}_{10}	0.164 538 57
ρ^{O}_{20}	−0.432 959 98
ρ^{O}_{22c}	0.029 803 192
ρ^{O}_{32c}	−0.184 800 385
(b) VRT(ASP-W)III	
α^{OO}	2.108 14
ρ^{O}_{10}	0.171 824
ρ^{O}_{20}	−0.429 006
ρ^{O}_{22c}	0.039 300 5
ρ^{O}_{30}	0.335 563
ρ^{O}_{32c}	−0.157 307

The total fitting time was reduced to approximately seven days on a Pentium III 733 MHz workstation. The values of the original ASP-W potential are given in Tables I–IV. The fitted parameters and correlation matrices for both fitted potentials are given in Tables V and VI. Readers will notice that most of the constants presented in these tables differ from those in the original ASP-W potential reported by Millot and Stone.[48] The differences are explained as follows: in the ASP-W computer code provided by Millot and Stone, the electrostatic multipole moments are expanded through quadrupole on the oxygens and dipole on the hydrogens, however, in the original Millot and Stone article, they reported moments expanded to octopole. Table I contains the numbers for the moments as actually found in the code. Additionally, the original article reported the unscaled induction terms. The correct terms (i.e., those used in the code), scaled to duplicate experimental measurements, are presented in Table IV.

III. RESULTS

A. VRT states

As shown in Tables VII and VIII, the $(D_2O)_2$ and $(H_2O)_2$ VRT sublevels in the ground vibrational state are reproduced quite well by both IPS, and many band origins and tunneling splittings are within the 0.02 cm^{-1} (600 mHz) uncertainty of the SWPS code for the given basis. The good agreement between theory and experiment is more apparent when one examines those states not actually included in the fit. As mentioned previously, we are currently unable to specify normal mode composition of the calculated excited vibrational states, so the vibrational assignments are based primarily upon the close proximity of predicted states to experimental states with appropriate symmetry. Figures 3 and 4 are plots of the $J=0$ states for VRT(ASP-W)II and experiment for both $(D_2O)_2$ and $(H_2O)_2$. The predicted VRT states of the original ASP-W potential have already been described.[22,23] As discussed in Papers I and II, the interchange splittings are too small to resolve in the energy scale

TABLE VI. The correlation matrix of the VRT(ASP-W)II fit (a) and the VRT(ASP-W)III fit (b).

(a) VRT(ASP-W)II

	ρ^{O}_{10}	ρ^{O}_{20}	ρ^{O}_{22c}	ρ^{O}_{32c}
ρ^{O}_{10}	1.00			
ρ^{O}_{20}	−0.94	1.00		
ρ^{O}_{22c}	0.77	−0.82	1.00	
ρ^{O}_{32c}	0.43	−0.14	−0.15	1.00

(b) VRT(ASP-W)III

	α^{OO}	ρ^{O}_{10}	ρ^{O}_{20}	ρ^{O}_{22c}	ρ^{O}_{30}	ρ^{O}_{32c}
α^{OO}	1.00					
ρ^{O}_{10}	−0.99	1.00				
ρ^{O}_{20}	0.644	−0.66	1.00			
ρ^{O}_{22c}	0.69	−0.71	0.96	1.00		
ρ^{O}_{30}	0.57	−0.57	−0.23	−0.17	1.00	
ρ^{O}_{32c}	−0.89	0.93	−0.40	−0.52	−0.74	1.00

of Figs. 3 and 4, so each triplet is drawn as a single line and given the label "1" or "2" (i.e., the $A_1^+/E/B_1^+$ triplet is labeled as "1").

Presented in Table VII and Fig. 4 are the predicted $J=0$ $(D_2O)_2$ VRT(ASP-W)II states and experimental results. Included in Table VII are the VRT(ASP-W)III results, as well as a comparison to the SAPT5st potential, recently published by Groenenboom *et al.*[24,25] Experimental data included in both of the potential determinations are denoted with an asterisk, and data included only in the VRT(ASP-W)III fit are denoted by a double asterisk. As seen both in the plot, and very clearly in Table VII, both VRT(ASP-W)II and VRT(ASP-W)III accurately describe those VRT data included in the fits, which includes the ground state tunneling splittings, the location of the 65 cm^{-1} band upper interchange triplet ("1" at 75 cm^{-1}), the location of the "1's" interchange triplet at 104 cm^{-1}, and the location of the 83 cm^{-1} band. However, the predicted ordering of the "1's" and "2's" of the 83 cm^{-1} band is reversed for both potentials; that is, VRT(ASP-W)II and III predict that "2" is closer to the ground state than "1," while the opposite has been found by experiment. This incorrect ordering is also predicted by the original ASP-W, but is correctly described by the "tuned" SAPT5st potential. We attempted to reverse this ordering by the adjustment of various combinations of the potential's constants, but were unable rectify this artifact. The source of this problem is currently unresolved, but could be due to overstructuring in the ASP-W potential form, or to the lack of intra- to intermolecular vibrational coupling [VRT(ASP-W)II and III assume rigid water monomers]. VRT(ASP-W)II and III both correctly predict the interchange triplet ordering of the 65 cm^{-1} band as well as the very large acceptor switching splitting (10.68 and 13.19 cm^{-1} predicted respectively, 15.8 cm^{-1} observed). VRT(ASP-W)II also models the tunneling splittings of the 90 cm^{-1} band with acceptable accuracy, although the predicted band center is approximately 10 cm^{-1} too low. Interestingly, portions of the band had been observed a number of years ago in our labo-

TABLE VII. Comparison of VRT(ASP-W)II and III predictions with SAPT5st and experimental results for $(D_2O)_2$ (cm^{-1}). Band Origin (1/2) is the band origin ν_0 of the 1's or 2's interchange triplet derived from the fit of the VRT spectra to the energy level expression. Interchange (1/2) is the interchange splitting of interchange triplet 1 or 2. Acceptor Switching is the absolute acceptor switching tunneling splitting. These splittings are illustrated in Fig. 1. Experimental data included in the VRT(ASP-W)II fit are marked with an asterix, and data included in the VRT(ASP-W)III fit are denoted with a double asterisk. Unobserved or data not yet analyzed are denoted with a dash.

	Ground State				Acceptor Wag (ν_8)			
	VRT(ASP-W)II	VRT(ASP-W)III	SAPT5st	Experiment	VRT(ASP-W)II	VRT(ASP-W)III	SAPT5st	Experiment
Band Origin (1)	0.00	0.00	0.00	0.00	82.82	83.76	89.82	82.64**
Band Origin (2)	1.77	1.65	1.69	1.77*	80.98	82.83	95.03	84.40**
Interchange (1)	0.04	0.02	0.0393	0.04*	0.16	0.06	0.15	0.13*
Interchange (2)	0.04	0.02	0.0385	0.04*	0.07	0.04	0.23	0.11*
Acceptor Switching	1.77	1.65	1.69	1.77*	−1.83	−0.93	5.21	1.76
	Donor Torsion (ν_{12})				Acceptor Twist (ν_{11})			
	VRT(ASP-W)II	VRT(ASP-W)III	SAPT5st	Experiment	VRT(ASP-W)II	VRT(ASP-W)III	SAPT5st	Experiment
Band Origin (1)	74.74	78.50	76.26	75.38*	83.08	93.46	93.78	92.91**
Band Origin (2)	64.06	64.93	60.13	59.59**	74.35	88.62	91.98	90.37**
Interchange (1)	0.53	0.08	0.10	0.33*	0.12	0.24	0.8407	0.43
Interchange (2)	0.06	0.02	0.11	0.27	0.67	0.32	0.9965	0.44
Acceptor Switching	10.68	13.57	16.13	15.81	8.74	4.84	1.80	2.54
	In-plane Bend (ν_6)				O–O Stretch (ν_7)			
	VRT(ASP-W)II	VRT(ASP-W)III	SAPT5st	Experiment	VRT(ASP-W)II	VRT(ASP-W)III	SAPT5st	Experiment
Band Origin (1)	103.94	108.93	107.32	104.24*	130.03	149.41	144.44	⋯
Band Origin (2)	129.80	132.86	140.50	⋯	137.62	153.71	150.88	⋯
Interchange (1)	0.38	0.05	0.6905	0.78*	5.64	0.13	1.399	⋯
Interchange (2)	3.97	0.27	0.1312	⋯	1.94	5.23	0.0175	⋯
Acceptor Switching	25.86	23.93	33.19	⋯	7.60	4.30	6.44	⋯

TABLE VIII. Comparison of VRT(ASP-W)II and III predictions with SAPT5st experimental results for $(H_2O)_2$ (cm^{-1}). See Table VII for details. Unlike the $(D_2O)_2$ data, the acceptor switching splitting has not been determined experimentally so the quoted experimental values are relative to the ground state. For example, for the ν_8 band, it has been confirmed that the acceptor switching splitting of vibrational mode is 10.2 cm^{-1} smaller than that of the ground state. (The predicted acceptor switching splitting in the ground state is 11.53 cm^{-1}.)

	Ground State				Acceptor Wag (ν_8)			
	VRT(ASP-W)II	VRT(ASP-W)III	SAPT5st	Experiment	VRT(ASP-W)II	VRT(ASP-W)III	SAPT5st	Experiment
Band Origin (1)	0.00	0.00	0.00	0.00	108.74	108.17	113.39	107.93
Band Origin (2)	11.86	10.67	11.18	11.18	99.50	99.93	110.00	97.71
Interchange (1)	0.60	0.36	0.72	0.75	2.44	1.14	2.60	2.95
Interchange (2)	0.59	0.39	0.65	0.65	−0.27	0.02	0.65	0.02
Acceptor Switching	11.86	10.67	11.18	11.18	−9.23	−8.24	−3.39	−10.20
	Donor Torsion (ν_{12})				Acceptor Twist (ν_{11})			
	VRT(ASP-W)II	VRT(ASP-W)III	SAPT5st	Experiment	VRT(ASP-W)II	VRT(ASP-W)III	SAPT5st	Experiment
Band Origin (1)	110.66	118.19	118.26	···	130.46	136.31	132.43	···
Band Origin (2)	69.76	73.28	64.52	64.44	106.55	121.02	120.97	120.19
Interchange (1)	4.12	1.54	3.05	1.11	0.70	2.40	4.99	···
Interchange (2)	1.33	0.397	1.72	2.54	6.84	4.92	10.36	9.39
Acceptor Switching	40.91	44.91	64.92	···	23.71	15.29	11.46	···
	In-plane Bend (ν_6)				O–O Stretch (ν_7)			
	VRT(ASP-W)II	VRT(ASP-W)III	SAPT5st	Experiment	VRT(ASP-W)II	VRT(ASP-W)III	SAPT5st	Experiment
Band Origin (1)	133.69	138.46	134.37	···	138.67	148.90	···	···
Band Origin (2)	150.83	152.65	148.22	~103.1	178.42	186.12	···	142.44
Interchange (1)	7.88	0.452	8.25	···	1.81	2.47	···	···
Interchange (2)	2.33	0.519	0.56	···	20.05	8.49	···	1.88
Acceptor Switching	17.14	14.19	22.08	···	39.74	37.22	···	···

ratory but were not attributed to a fundamental vibration of $(D_2O)_2$. Prompted in part by the predictions given here, one of us (L.B.) reinvestigated the original spectra and discovered the vibration at 90 cm^{-1} within this data set. These two band centers were then used in the fit for VRT(ASP-W)III, which accordingly shows an improvement in their predicted location.

Comparison of the VRT(ASP-W) fits with SAPT5st shows that the two agree quite well. The SAPT5st potential makes remarkably accurate predictions of tunneling splittings and band origins of $(D_2O)_2$, considering that it was only "tuned" to fit the $(H_2O)_2$ acceptor tunneling splitting.[24,25] However, it predicts a band origin for the "1's" that is over 7 cm^{-1} too high, and a band center for the "2's"

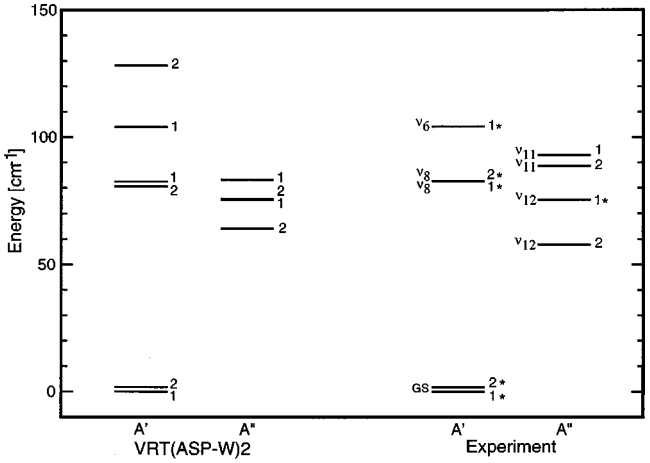

FIG. 3. The ordering of the $J=0$ VRT states below 150 cm^{-1} of $(D_2O)_2$ water dimer calculated using VRT(ASP-W)II, compared to measured $J=0$ states. Shown are the upper and lower A/E/B interchange triplets segregated by A′ or A″ vibrational symmetry (Fig. 1). On the scale of this plot, the individual interchange triplets are only partially resolvable, therefore, the symmetry labels for individual levels have been omitted for clarity. The asterisk denotes states included in the fit. Vibrational assignments to experimental data are, GS-ground state, ν_6-in-plane bend, ν_7-O–O stretch, ν_8-acceptor wag, ν_{11}-acceptor twist, and ν_{12}-donor torsion. See Secs. I and II for explanation of these assignments. Vibrational assignment of the predicted states is not implemented in the fitting program.

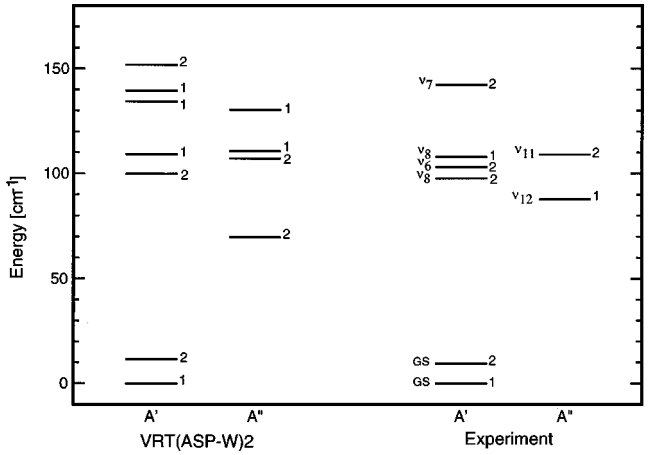

FIG. 4. The ordering of the $J=0$ VRT states below 180 cm^{-1} of $(H_2O)_2$ calculated using VRT(ASP-W)II are compared to measured $J=0$ states. See Fig. 3 for details.

TABLE IX. A comparison of the ground-state properties of $(D_2O)_2$ and tunneling barriers of the IPS.

	Ground-State Water Dimer Properties					
	Expt.[a]	VRT(ASP-W)II$_{vib}$[b]	VRT(ASP-W)II$_{eq}$[b]	VRT(ASP-W)III	*Ab initio*[c]	ASP-W[d]
D_e [kcal/mol]	5.40(0.5)	···	4.85	4.92	5.05	4.69
D_0 [kcal/mol]	3.66(0.5)	3.40	···	3.47	···	···
R_{OO} [A]	2.976(0.00,−0.03)	2.99(20)	2.952	···	2.953	2.972
θ_a [deg]	57(10)	45.1(3)	48.5	···	56.0	64.6
θ_d [deg]	51(10)	58.9(2)	49.9	···	59.1	44.5
A [GHz]	124.9	121.9	115.3	···	···	···
(B+C)/2 [GHz]	5.433	5.268	5.473	···	···	···
(B–C) [BHz]	33.11	25.81	13.91	···	···	···
μ_a [Debye]	2.60	2.51(10)	2.70(10)	···	···	···

	Tunneling Barriers [cm^{-1}]				
	VRT(ASP-W)II$_{vib}$[b]	SAPT-5st	*Ab initio*[e]	*Ab initio*[f]	ASP-W
Switching [cm^{-1}]	154	222	164	175	277
Interchange [cm^{-1}]	229	248	192	204	149
Bifurcation [cm^{-1}]	430	685	563	476	484

[a]The *B* and *C* rotational constants and dipole moment were measured by microwave and Stark experiments of Odutola and Dyke (Ref. 53). Using these data in conjunction with measurements for other dimer isotopes, they derived the equilibrium structure parameters R_{OO}, θ_d, and θ_a using a constrained model (rigid monomers). The structure parameters are defined in Fig. 2. The *A* rotation constant is estimated from the far-IR measurements of Karyakin *et al.* (Ref. 35). The equilibrium and zero-point dissociation energies are from the thermal conductivity experiments of Curtiss *et al.* (Ref. 58).

[b]The VRT(ASP-W) vibrationally averaged structure was determined by the DQMC method. The rotational constants were calculated using fixed monomer geometries of $\angle$HOH=104.52° and R_{OH}=0.9572 A and masses D=2.014 102 2 and O=15.994 915. Note the excellent agreement between the experimental observables, A, $(B+C)/2$, $B-C$, and μ_a (dipole moment projected on the principal axis), which are model independent, and the vibrationally averaged values predicted by VRT(ASP-W).

[c]High level *ab initio* calculations of Mas and Szalewicz using Symmetry Adapted Perturbation Theory (Ref. 56).

[d]The original ASP-W potential of Millot and Stone (Ref. 48). The principal tunneling barriers of the VRT(ASP-W) and ASP-W surfaces are compared to SAPT-5st results, as well as to *ab initio* results of Smith *et al.* (Ref. 63) and Wales (Ref. 65). The VRT(ASP-W) and ASP-W barriers were found with the Orient program (Ref. 61). *Ab initio* calculations were performed at the MP2 level with counterpoise corrections to improve accuracy.

[e]Reference 63.

[f]Reference 65.

that is over 10 cm^{-1} too high. Both of these band origins are predicted to ca. 2 cm^{-1} by VRT(ASP-W)II and III. It should also be noted that VRT(ASP-W)III and SAPT5st make strikingly similar predictions for band origins that have yet to be observed experimentally, namely, that for ''2's'' of the in-plane bend, and those for both the ''1's'' and ''2's'' of the O–O Stretch.

The match between $(H_2O)_2$ states predicted by VRT(ASP-W)II and experiment is reasonably good, considering that no $(H_2O)_2$ VRT data were actually used in the fit (see Table VIII and Fig. 4). There is a good correspondence between the VRT(ASP-W)II prediction and both of the interchange triplet band origins and interchange splittings of the ν_8 acceptor wag. An experimental observation not correctly described in the prediction is the ''2's'' sub-band of the ν_6 in-plane bend at 103 cm^{-1}. However, this transition has also proven a challenge for other potentials, including SAPT-5st, and will be better understood once more data are available. VRT(ASP-W)III improves substantially on virtually all of the $(H_2O)_2$ predictions relative to versions I and II. It marks an improvement over SAPT5st in terms of the band origin of the ''1's'' and ''2's'' of the acceptor wag (108.17 and 99.93 cm^{-1}, compared to 113.39 and 110.00 cm^{-1} for SAPT5st, and 107.93 and 97.71 for the experiment), as well as the acceptor switching (−8.24 cm^{-1}, compared to −3.39 cm^{-1} for SAPT5st, and −10.20 for the experiment). However, SAPT5st provides a more accurate prediction for the band origin of the ''2's'' of the donor torsion [64.52 cm^{-1}, compared to 73.28 cm^{-1} for VRT(ASP-W)III, and 64.44 cm^{-1} for the experiment], but this is expected, since SAPT5st was ''tuned'' to the $(H_2O)_2$ data itself.

B. Ground-state structure

The ground-state structural properties of $(H_2O)_2$, $(D_2O)_2$, and partially deuterated isotopes have been previously determined by Odutola and Dyke from their microwave spectroscopy results.[53] Their $(D_2O)_2$ rotational constants, dipole moment, and equilibrium structural parameters are presented in Table IX. The large error bars on the θ's reflect the uncertainties due to the flat and anharmonic nature of the potential and the limited data set used in that determination. The R_{OO} is an upper bound to the equilibrium oxygen–oxygen separation. In Odutola and Dyke's estimation of the effect of anharmonicity, using the force constants of the dimer calculated by Curtiss and Pople at the HF/6-31G* level,[54] the maximum correction to the distance should be 0.03 Å so that 2.946 Å$\leqslant R_{OO} \leqslant$2.976 Å. There is, however, considerable doubt as to the accuracy of this structural determination, again reflecting the limited available data. A number of high level *ab initio* studies of the water dimer find R_{OO} to be shorter, in the range 2.89–2.95 Å. Additionally, the values of the θ's are sensitive to the level of theory and basis set. As an example, Xantheas[55] found that at the HF/aug-cc-pVDZ level, the equilibrium structure is R_{OO}=3.032 Å, θ_a=46.2°, and θ_d=57.8°. At the MP2/aug-cc-pVDZ level these parameters change to R_{OO}=2.920 Å,

$\theta_a = 49.3°$, and $\theta_d = 52.0°$, and at the MP/aug-cc-pVTZ level, $R_{OO} = 2.898$ Å, $\theta_a = 49.0°$, and $\theta_d = 52.2°$.

For comparison, the ground-state equilibrium and vibrationally averaged properties of VRT(ASP-W)II are shown in Table IX. Included are D_0 and an estimate of D_e of VRT(ASP-W)III. In the original ASP-W surface, the dimer equilibrium structure does not have a plane of symmetry (C_s) as the hydrogen-bonded proton lies slightly off of the mirror plane (C_l). Millot and Stone[48] considered this to be an artifact, as experimental evidence is strongly in favor of a minimum structure with a plane of symmetry. The minimum of VRT(ASP-W)II does in fact have C_s symmetry. For the equilibrium structure of VRT(ASP-W)II, R_{OO} is essentially in perfect agreement with the best *ab initio* predictions[56] and the two θ angles are within the (large) error bars of Odutola and Dyke. We have also calculated expectation values of $\langle R_{OO} \rangle$, $\langle \theta_a \rangle$, and $\langle \theta_d \rangle$ in the ground states of both $(H_2O)_2$ and $(D_2O)_2$ by diffusion Quantum Monte Carlo methods.[57] We find that the effective potentials for these three degrees of freedom are strongly anharmonic and very flat near the minimum energy configuration, as shown in Fig. 5. The expectation values for both angles differ from their equilibrium values by about 8°, and $\langle R_{OO} \rangle$ is almost 0.04 Å larger than the equilibrium value of 2.952 A. We also find that the sum and difference of the *B* and *C* rotational constants are in good agreement with the experimental values. The *A* constant is not as close to experiment as are *B* and *C*, but is quite reasonable considering the difficulty in precisely determining this quantity. Presently, the three best measurements of *A* are 125.8 GHz,[33] 124.9 GHz,[35] and 125.6 GHz,[39] while the vibrationally averaged value from VRT(ASP-W)II is 121.9 GHz.

The dipole projection on the *A*-axis is a combination of the monomer permanent moments and induced moments. We can estimate μ_a as

$$\mu_a = \mu_0[\cos\theta_a + \cos\theta_d](1 + 2\alpha R^{-3}),$$

where μ_0 is the permanent monomer dipole (1.855 a.u.), R is the separation of polarizability sites (R_{OO} for these potentials), and α is the isotropic polarizability [$\alpha = 1/3(\alpha_{xx} + \alpha_{yy} + \alpha_{zz}) = 1.470$ A^3]. This equation only accounts for dipole-induced dipoles and neglects contributions from higher-order moments, as well as effects of the slightly anisotropic nature of the polarizability. Olthof, van der Avoird, and Wormer estimate that this is accurate to about 0.1 D.[17] Both the calculated equilibrium and vibrationally averaged μ_a's reproduce the experimental values within the stated uncertainties.

In addition to the structural properties of the ground state, we can also compare the zero-point and equilibrium dissociation energies (D_0 and D_e, respectively) determined in thermal conductivity experiments of Curtiss, Frurip, and Belander.[58] D_0 is the measured property; D_e was estimated by adding the zero-point energy calculated at the HF/4-21 Glevel of theory by Curtiss and Pople.[54] The values they reported for $(D_2O)_2$ are $D_0 = -3.66$ kcal mol^{-1} and $D_e = -5.40$ kcal mol^{-1}. Since it is known that the water dimer potential is very anharmonic, it is generally agreed that the magnitude of this D_e is an upper bound. High level *ab initio* calculations obtain $D_e \approx -4.7$ to -5.1 kcal mol^{-1}.[3,26,59,60] The D_0 and D_e of both VRT(ASP-W)II and III are well within the range of the best theoretical estimates.

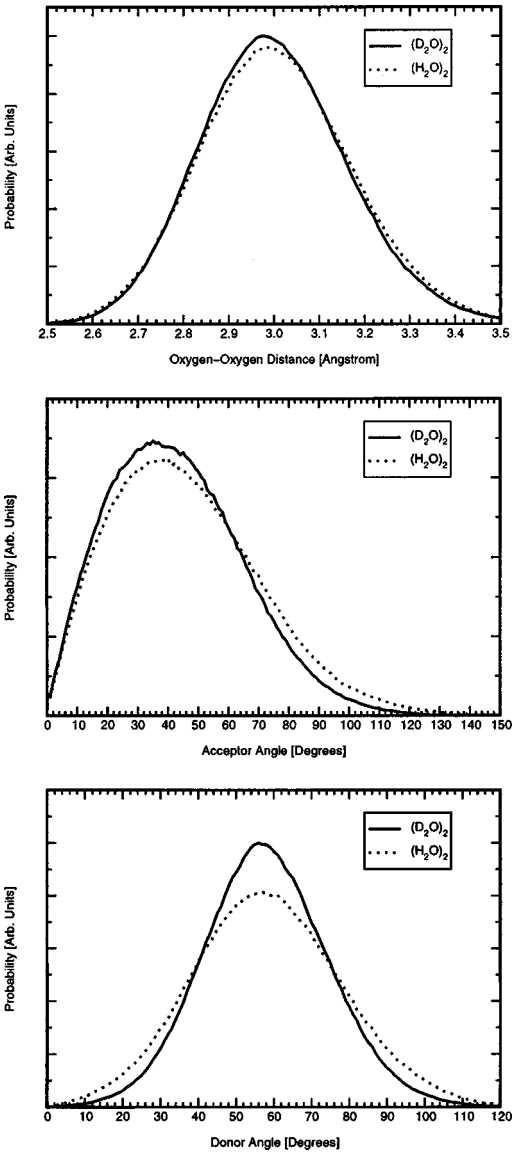

FIG. 5. Diffusion Quantum Monte Carlo probability plots for $(D_2O)_2$ and $(H_2O)_2$ on the VRT(ASP-W)II IPS. Expectation values for R_{OO}, θ_a, and θ_d are shown in Table IX.

C. Second virial coefficients

To further characterize VRT(ASP-W)II, we have calculated the temperature dependent second virial coefficients (SVC). The SVC are calculated as the sum of the classical component

$$B_{cl}(T) = -\frac{1}{2}\int \langle e^{-U_{12}/kT} - 1 \rangle_{\omega_1\omega_2} dr,$$

and first-order quantum corrections

$$B_q(T) = \frac{\hbar}{24(kT)^3}\left[\frac{\langle F^2 \rangle_0}{M} + \sum_\alpha \frac{\langle T_\alpha^2 \rangle_0}{I_{\alpha\alpha}}\right],$$

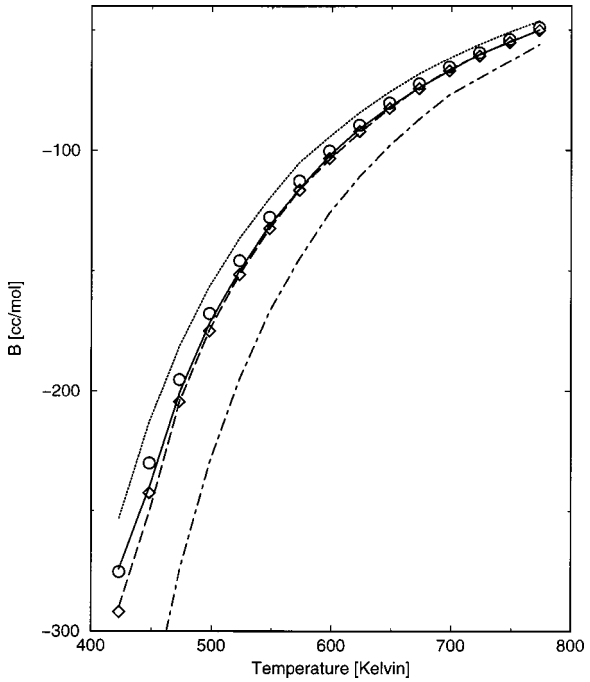

FIG. 6. The temperature dependent second virial coefficients calculated from VRT(ASP-W)II with quantum corrections, for D_2O (— — —) and H_2O (——), ASP-W with H_2O (···), TIP4P with H_2O (-·-·-), and the H_2O (○) and D_2O (□) experimental data of Kell *et al.* (Ref. 62) *B*, the second virial coefficient, is the deviation of the density of steam from the idea gas law.

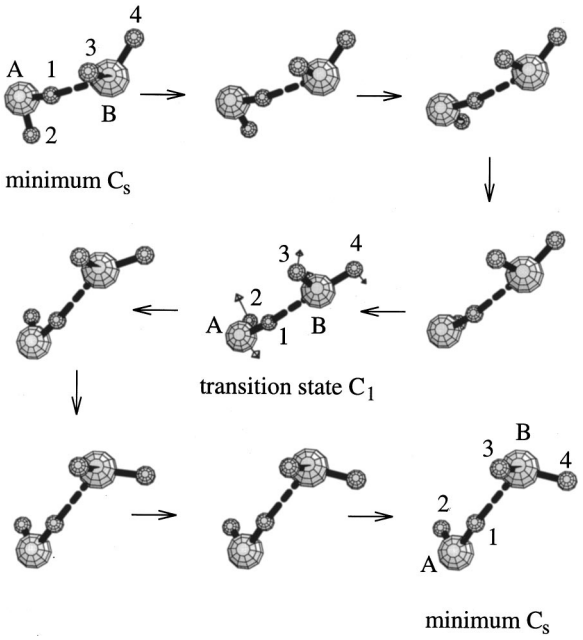

FIG. 7. Acceptor switching tunneling path for $(H_2O)_2$ calculated at the DZP+diff/BLYP level (Ref. 64). Figure courtesy of Prof. David Wales.

where $\langle F^2 \rangle$ and $\langle T^2 \rangle$ are the mean-square force and torque, respectively, experienced by one molecule due to the interaction with another and U_{12} is the pair potential energy. The sum of α is over the principal axis of the molecule, M is the molecular mass, T_α is the torque about the α axis, and $I_{\alpha\alpha}$ is the moment of inertia associated with this axis. As the SVC serve as a measure of the volume of the potential well in addition to the well depth, they are particularly important since the error bars on the experimentally determined D_0 and D_e are so large.

To calculate $B(T)$, we used the Orient program.[61] Integration was performed using the Monte Carlo scheme with R varied from 0–30 bohr in increments of 0.5 bohr. The potential was integrated over a total of 10 000 points. By measuring the convergence of $B(T)$, versus the number of integration points, we estimate that the calculated values are accurate to about ±2%. The data are plotted in Fig. 6. As seen in this plot, the predicted SVCs of VRT(ASP-W)II are essentially identical to the best experimental data[62] available for both $(H_2O)_2$ and $(D_2O)_2$. We have not repeated this calculation for VRT(ASP-W)III, but a similar result is expected due to the overall similar spectroscopic predictions between it and VRT(ASP-W)II.

D. Tunneling pathways

As discussed earlier, the water dimer undergoes three classes of tunneling motions among the eight identical global minimum structures on the 6D IPS. These motions are acceptor switching (AS), interchange (I), and bifurcation (B), and are manifested as a hierarchy of splittings in high resolution microwave and infrared spectra. A description of these rearrangements and their effects on the VRT spectra were given in detail in Paper I.[18]

In 1990, Smith *et al.*[63] reported a number of stationary points on the water dimer surface calculated at MP2/6-31 +G(d,p) and higher levels of theory. The three lowest first-order stationary point structures they found are believed to correspond to transition states of the rearrangement pathways.[63] Recently, Wales[64,65] traced out these tunneling motions on a MP2/DZP+diff surface using the eigenvector-method following.[66] He found that acceptor switching proceeds by a methylaminelike pathway whereby the donor rotates about the hydrogen-bond axis, while the acceptor simultaneously flips up (see Fig. 7). In interchange, the monomers rotate in a geared motion where the transition state has a *trans*-configuration (see Fig. 8). In bifurcation, both monomers flip through a bifurcated transition state without breaking the C_s symmetry (see Fig. 9). The predicted transition state structures and relative energies of Smith *et al.* and Wales are compared in Table IX.

To analyze the VRT(ASP-W)II surface, we carried out an extensive search for first-order stationary points using the Orient program, similar to the analysis of the ASP-W surface conducted by Millot *et al.*[67] and the VRT(ASP-W) surface by Fellers *et al.*[23] As seen in Table IX, the acceptor switching, interchange, and bifurcation tunneling barriers of VRT(ASP-W)II agree well with the *ab initio* predictions of Smith *et al.* and Wales. In particular, note that VRT(ASP-W)II has corrected the reversed ordering of the acceptor switching and interchange barriers present in the original ASP-W. Comparison is also made to the SAPT5st tunneling barriers calculated by Mas *et al.*[27] for $(H_2O)_2$ even though VRT(ASP-W)II is an explicit $(D_2O)_2$ potential.

As in Wales' study, we also traced out the VRT(ASP-W)II tunneling pathways. We first located the first-order sta-

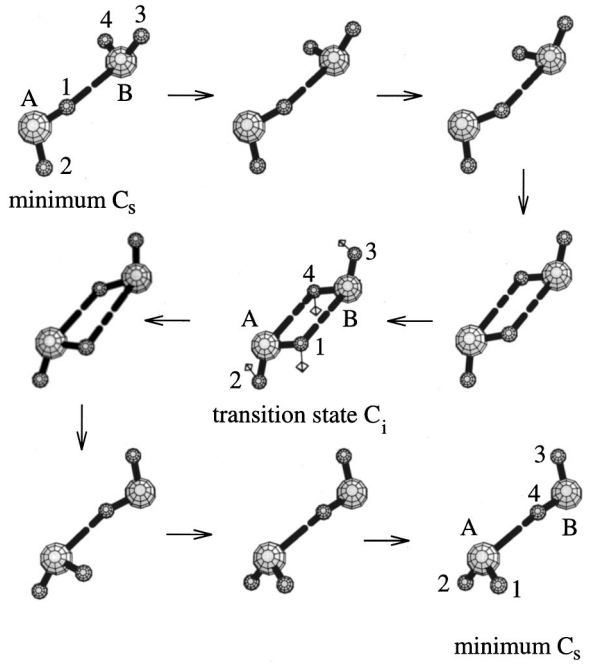

FIG. 8. *Trans*-interchange tunneling path for $(H_2O)_2$ calculated at the DZP+diff/BLYP level (Ref. 64). Figure courtesy of Prof. David Wales.

tionary points on ASP-W and VRT(ASP-W)II. We then verified the order of the stationary point by inspecting the Hessian, where all real normal mode frequencies indicate a minimum and one, only one, imaginary normal mode frequency indicates a first-order stationary point. Tunneling pathways were determined by following the minimum energy pathways from a selected transition state to one of the global minima. The pathway from a transition state is determined by adding or subtracting a small displacement along the normal mode corresponding to the unique imaginary frequency. All searches employed the eigenvector following method available in the Orient program, and the stationary point geometries are given in Fig. 10. The interchange and bifurcation motions were essentially identical to Wales' findings. The acceptor switching motion appears to be slightly different in that on the VRT(ASP-W)II surface, the acceptor flips up before the donor begins its methylamine like rotation about the hydrogen bond. In Wales' description, the motion of the two monomers appears to be concerted. Additionally, we found that along the acceptor switching tunneling coordinate, the VRT(ASP-W)II surface passes through three nearly identical first-order transition states. It is our belief that these two additional structures are an indication that the surface has small bumps or ripples near the acceptor switching tunneling barrier maximum. These findings are essentially identical to our earlier surface, VRT(ASP-W).[23]

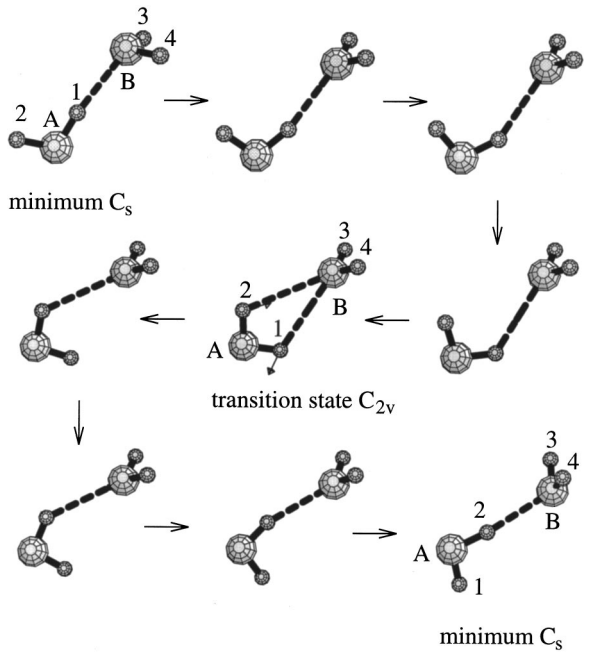

FIG. 9. Bifurcation tunneling path for $(H_2O)_2$ calculated at the DZP+diff/BLYP level (Ref. 64). Figure courtesy of Prof. David Wales.

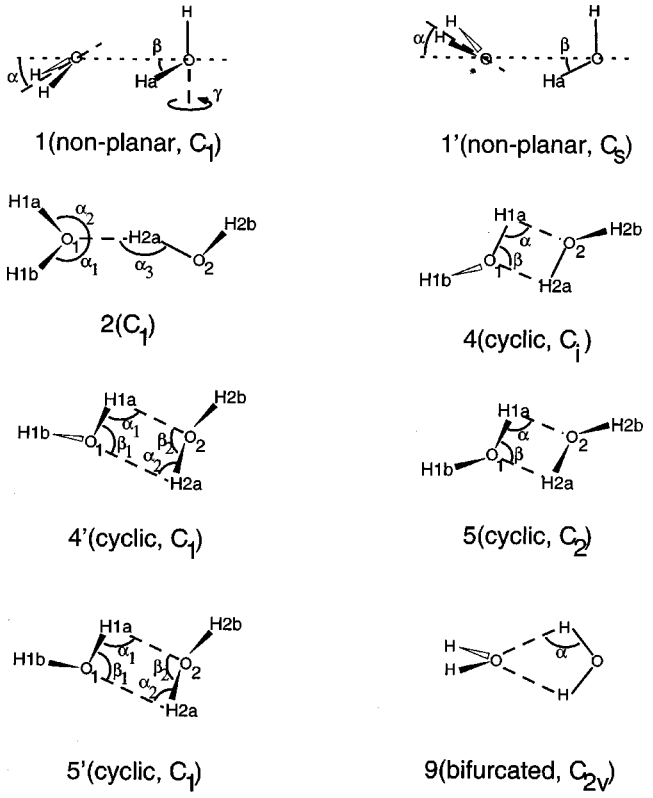

FIG. 10. Ground-state and first-order stationary point structures of ASP-W and VRT(ASP-W)II. The labeling scheme is reproduced from Ref. 64.

To quantify the rearrangement pathways and to give some useful insight, we have measured the integrated pathlength. The path length is defined as $S=\int ds$, the integrated arc length in the 18-dimensional nuclear configuration space. S was calculated as a sum over the eigenvector-following steps:

$$S=\sum_{\text{steps}}\left(\sum_i \Delta Q_i^2\right)^{1/2},$$

where ΔQ_i is the step for the nuclear Cartesian coordinate Q_i and the outer sum is over all the eigenvector-following steps. Both S and the Q_i have dimension of length: no mass weighting is involved. To further aid in our understanding, we have plotted the integrated pathways versus the binding energy at each step. These plots, which we shall call "inte-

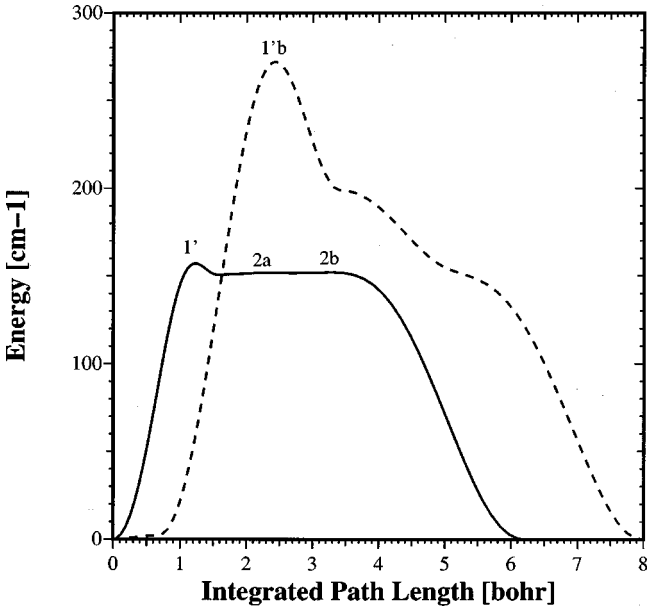

FIG. 11. IRP plots of the acceptor switching pathways of the ASPW (dotted lines) and VRT(ASP-W)II (solid lines) potentials. The VRT(ASP-W)II potential begins at the ground state equilibrium energy (D_e) of 20.585 kJ/mol. The ASPW IRP is normalized to the same starting energy to emphasize the difference in the tunneling pathways. The numbered annotations refer to the first-order stationary points found in Fig. 10.

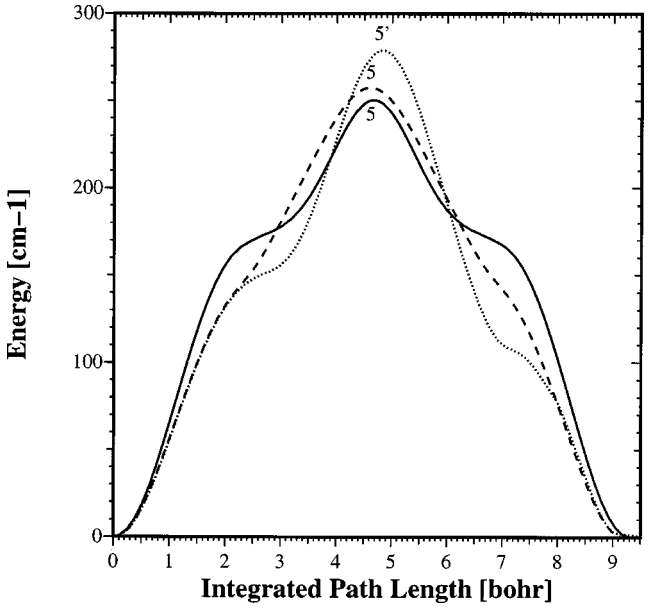

FIG. 13. IRP plots of the *cis*-interchange pathways of the ASPW (dotted lines) and VRT(ASP-W)II (solid lines) potentials, with the same energy normalization for the ASPW IRP and the same reference to the numbered annotations.

grated rearrangement pathway'' (IRP) plots, provide an effective 1-dimensional picture of a multidimensional tunneling barrier. The IRP plots are shown in Figs. 11–14 where we compare the pathways of ASPW and VRT(ASP-W)II. In the acceptor switching pathways of Fig. 11, both ASPW and VRT(ASP-W)II have a tunneling motion that generally proceeds as follows. Moving in the forward direction along the integrated pathway and starting with the ground state, the acceptor flips up to achieve structure 1′. Then the donor twists 180° about the hydrogen bond, passing through one or more geometries like structure 2 on its way back to the ground state. The VRT(ASP-W)II IRP passes through three first-order stationary points of similar energy: 1′, 2a, and 2b. ASPW only possesses 1′ as a first-order stationary point. ASPW also passes through structures very similar to 2a and 2b and are seen as shoulders on the IRP plot at 3.5 and 5.2 bohr. These latter two geometries are not transition states but

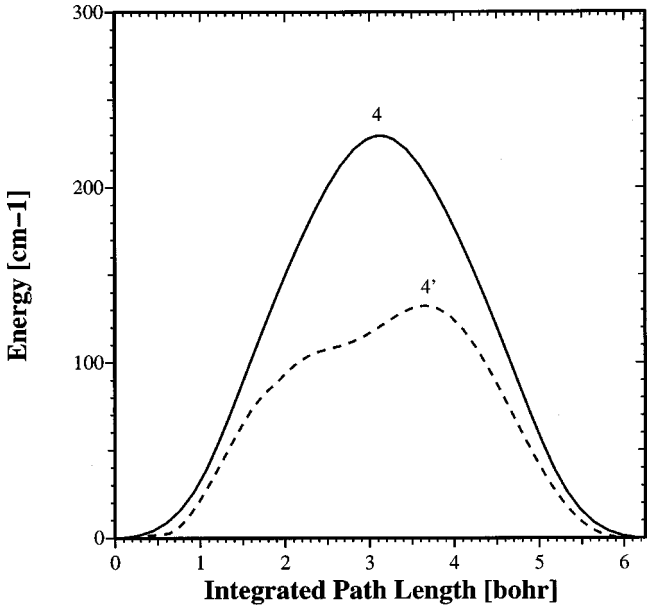

FIG. 12. IRP plots of the *trans*-interchange pathways of the ASPW (dotted lines) and VRT(ASP-W)II (solid lines) potentials. Again, the ASPW IRP is normalized to the same starting energy to emphasize the difference in the tunneling pathways, and the numbered annotations refer to the first-order stationary points found in Fig. 10.

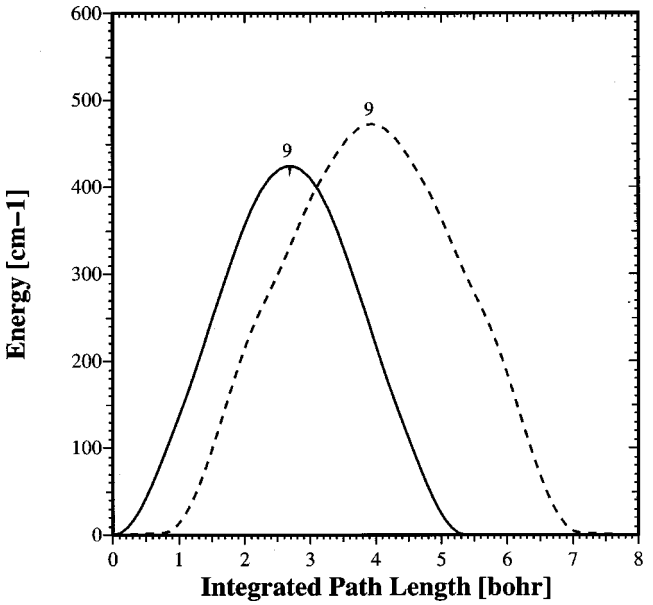

FIG. 14. IRP plots of the bifurcation pathways of the ASPW (dotted lines) and VRT(ASP-W)II (solid lines) potentials, with the same energy normalization for the ASPW IRP and the same reference to the numbered annotations.

may be higher-order stationary points. The maximum barrier heights for ASPW and VRT(ASP-W)II are 3.317 and 1.880 kJ/mol, respectively, and the integrated pathlengths are 8.005 and 6.200 bohr, respectively.

Regarding the interchange pathways, there are two types that are distinguished by the geometry of the transition state (see Fig. 12). The more facile rearrangement passes through a *trans*-cyclic geometry (e.g., structures 4 and 4′ of Fig. 10) while the more hindered motion possesses a transition state with a *cis*-geometry (e.g., structures 5 and 5′ of Fig. 10). With the *trans*-interchange mechanism of VRT(ASP-W)II, both monomers rotate in a concerted geared fashion that is symmetric about the transition state. The *trans*-interchange pathway with ASPW, however, is not symmetrical. Moving in the positive direction along the integrated pathlength (see Fig. 12), the geometry on the shoulder at 2.2 bohr is similar to 1′ with $\alpha \approx 90°$ and the transition state is the nonsymmetrical cyclic *trans*-structure 4′.

The *cis*-interchange pathways found on the ASP-W and VRT(ASP-W)II surfaces are quite convoluted. The VRT(ASP-W)II pathway has a symmetric *cis*-cyclic structure 5 at the transition state (see Fig. 13). The geometries of the shoulders at 2.5 and 6.5 bohr are very similar to structure 2. The ASP-W surface actually has two *cis*-interchange pathways. The pathway with the lower barrier is similar to the VRT(ASP-W)II pathway in the way that the monomers twist in a concerted motion as they pass over the barrier. The other pathway with the higher barrier has a transition state with an asymmetric *cis*-cyclic structure 5′, the geometry of the shoulder at 2.7 bohr similar to structure 2, and the shoulder at 7.2 bohr similar to 1′ with $\alpha \approx 90°$.

Compared to the acceptor switching and interchange pathways, the bifurcation pathway is unremarkable (Fig. 14). The IRP plot shows that VRT(ASP-W)II has a smaller barrier height and shorter integrated pathlength than ASPW. Based upon *ab initio* calculations of the bifurcation transition state, the barrier of VRT(ASP-W)II is probably too small. Bifurcation tunneling is manifested as a very small shift of the E states relative to the A/B states, which is too small to fit with quantitative accuracy in our calculation. Because this shift is not actually included in the fit, the bifurcation barrier is unconstrained. To test that the barrier on the VRT(ASP-W)II surface is reasonable, we calculated the VRT states with basis large enough ($j_{\max}=12$) to converge the ground state E-levels with reasonable accuracy and find that the difference between the calculated bifurcation shift versus the experimental bifurcation shift is $<0.001\ \mathrm{cm}^{-1}$.

E. Larger cluster characteristics

To further examine VRT(ASP-W)II, we have computed both equilibrium and vibrationally averaged ground-state structures, D_e, and D_0 for cyclic D_2O trimers and tetramers, which have been extensively studied by terahertz laser spectroscopy.[68–70] The predictions were calculated by using DQMC on a trimer (tetramer) IPS constructed by pairwise addition of the dimer potentials, followed by computing the self-consistent, iterated, *n*-body induction. As shown in Table X, good agreement is found with both *ab initio* and experimental results, and again a significant improvement relative to ASP-W is found, which generally produced O–O distances that were too long. Once again, it should be noted that the above calculations were not repeated for VRT(ASP-W)III due to the fact that the two IPS's are so similar. Effective pair potentials, such as TIP4P, are not able to reproduce the cluster features, yielding rather short O–O distances and binding energies that are too large. That a dimer potential such as VRT(ASP-W)II does so well in calculating properties of larger clusters is not entirely unexpected, as the dominant *n*-body force is induction (polarization), which is explicitly and rigorously treated by the polarizable VRT(ASP-W)II potential. In contrast, effective pair potentials parameterize the many-body forces in an average way according to bulk properties and so are unable to simultaneously describe both small clusters and the bulk. Moreover, the spectroscopic SAPT5 potentials[24,25] do not include these effects, and thus are not capable of describing larger clusters (or the liquid) without further modification. Our treatment does neglect the smaller three-body exchange and dispersion interactions, which must ultimately be included in a fully rigorous treatment.

TABLE X. Geometrical parameters and energies for the D_2O trimer and tetramer cyclic ground state. Pairwise and iterated *n*-body induction forces are calculated to first-order, that is, induction is estimated by one pass through the self-consistency loop. Induction for VRT(ASP-W)II is iterated to self-consistency. Vibrationally averaged structures and energies are computed by the DQMC method. D_e and D_0 specify the energy required to break all hydrogen bonds. Distances are in angstroms and energies in kcal/mol.

	Expt.[a]	VRT(ASP-W)II	ASP-W	TIP 4P[b]	*Ab initio*[c]
Trimer					
Avg. $R_{OO(eq)}$	⋯	2.776	2.881	2.764	2.804
Avg. $R_{OO(vib)}$	2.845	2.86(12)	⋯	⋯	
D_e	⋯	16.05	14.82	16.73	16.68
D_0	⋯	11.34(3)	⋯	⋯	
Tetramer					
Avg. $R_{OO(eq)}$	⋯	2.703	2.866	2.730	2.771
Avg. $R_{OO(vib)}$	2.789	2.78(1)	⋯	⋯	
D_e	⋯	28.761	24.33	27.87	28.57
D_0	⋯	21.34(3)	⋯	⋯	

[a]Reference 74.
[b]Reference 42.
[c]MP2/aug-cc-pVDZ with counterpoise correction (Ref. 75).

IV. DISCUSSION

In the course of producing these new VRT(ASP-W)II and III surfaces, we have retained the desirable features of its predecessor,[23] VRT(ASP-W), while significantly improving the accuracy of the induction energy by iterating to self-consistency. This improvement will give a more accurate description of the three-, four-, etc. terms, which are crucial to properly describing bulk water, one of the ultimate goals of this research. These new IPS afford an excellent reproduction of experimental data, including $(D_2O)_2$ VRT spectra, ground-state term values and dipole moments, dissociation energies, second virial coefficients, and larger cluster geometries. VRT(ASP-W)II does not model the known $(H_2O)_2$ VRT spectra as well as that for $(D_2O)_2$. but the results are nevertheless satisfying, considering that only $(D_2O)_2$ VRT data were incorporated into the fitting procedure. With only a

few new experimentally observed transitions added to the fit, VRT(ASP-W)III shows a marked improvement in terms of the ability to reproduce $(H_2O)_2$ spectra. However, the two new surfaces are otherwise similar, although the extensive and computationally expensive tests performed on version II were not explicitly repeated for version III.

The principal approximation implicit in the VRT(ASP-W) potential form is the constraint of freezing water monomer properties to equilibrium values. It is known that the donor O–H bond actually elongates slightly ($<1\%$) upon hydrogen bond formation, accompanied by smaller changes in the bond angle.[55,71] Although these subtle effects must eventually be included to obtain a ''perfect'' water dimer potential, to do so requires a complete 12D treatment of the VRT dynamics and potential surface, which requires more computing power than is currently available. Preliminary explorations indicate that the main effects of including monomer nonrigidity involve some reduction in the acceptor switching splitting and a small (~ 0.1 kcal mol^{-1}) increase in D_e. In any case, we expect the effects of monomer nonrigidity on the fitted potential to be relatively minor;[71] VRT(ASP-W)II is clearly quite close to the ''exact'' water dimer potential, and the refined version, VRT(ASP-W)III shows still higher accuracy. Moreover, as computational power continues to increase, it will ultimately become possible to determine the small exchange-repulsion and dispersion contributions to the many-body interactions[72] that are operative within aggregates of water molecules, as well as to further refine subtle features of the dimer potential by comparing results computed rigorously from this dimer potential with the precise VRT data measured for the water trimer, tetramer, pentamer, and hexamer. Considering that the neglected many-body terms constitute a small fraction of the condensed-phase water force field,[73] this rigorous determination of the polarizable water dimer potential surface implies that a truly rigorous molecular description of the force fields of solid and liquid water may be close at hand.

ACKNOWLEDGMENTS

This investigation was supported by the Experimental Physical Chemistry program of NSF and the CNRS-NSF Cooperative Grant Program. The authors would like to thank Serena Anderson for helpful discussions about the experimental data.

[1] F. N. Keutsch and R. J. Saykally, Proc. Natl. Acad. Sci. U.S.A. **98**, 10533 (2001).
[2] R. Car and M. Parrinello, Phys. Rev. Lett. **55**, 2471 (1985).
[3] S. Rybak, B. Jeziorski, and K. Szalewicz, J. Chem. Phys. **95**, 6576 (1991).
[4] M. Boero, K. Terakura, T. Ikeshoji, L. Chee Chin, and M. Parrinello, Phys. Rev. Lett. **85**, 3245 (2000).
[5] M. Boero, K. Terakura, T. Ikeshoji, C. C. Liew, and M. Parrinello, J. Chem. Phys. **115**, 2219 (2001).
[6] S. S. Xantheas, J. Chem. Phys. **100**, 7523 (1994).
[7] M. L. Klein and R. A. Aziz, *Inert Gases: Potentials, Dynamics, and Energy Transfer in Doped Crystals* (Springer, Berlin, 1984).
[8] R. J. Le Roy and J. M. Hutson, J. Chem. Phys. **86**, 837 (1987).
[9] H. C. Chang, F. M. Tao, W. Klemperer, C. Healey, and J. M. Hutson, J. Chem. Phys. **99**, 9337 (1993).
[10] M. L. Dubernet and J. M. Hutson, J. Chem. Phys. **99**, 7477 (1993).
[11] J. M. Hutson, J. Chem. Phys. **96**, 6752 (1992).
[12] J. M. Hutson, J. Phys. Chem. **96**, 4237 (1992).
[13] R. C. Cohen and R. J. Saykally, J. Phys. Chem. **94**, 7991 (1990).
[14] R. C. Cohen and R. J. Saykally, J. Chem. Phys. **98**, 6007 (1993).
[15] C. A. Schmuttenmaer, R. C. Cohen, and R. J. Saykally, J. Chem. Phys. **101**, 146 (1994).
[16] M. J. Elrod and R. J. Saykally, J. Chem. Phys. **103**, 933 (1995).
[17] E. H. T. Olthof, A. van der Avoird, and P. E. S. Wormer, J. Chem. Phys. **101**, 8430 (1994).
[18] L. B. Braly, J. D. Cruzan, K. Liu, R. S. Fellers, and R. J. Saykally, J. Chem. Phys. **112**, 10293 (2000).
[19] L. B. Braly, K. Liu, M. G. Brown, F. N. Keutsch, R. S. Fellers, and R. J. Saykally, J. Chem. Phys. **112**, 10314 (2000).
[20] C. Leforestier, J. Chem. Phys. **101**, 7357 (1994).
[21] C. Leforestier, L. B. Braly, L. Kun, M. J. Elrod, and R. J. Saykally, J. Chem. Phys. **106**, 8527 (1997).
[22] R. S. Fellers, L. B. Braly, R. J. Saykally, and C. Leforestier, J. Chem. Phys. **110**, 6306 (1999).
[23] R. S. Fellers, C. Leforestier, L. B. Braly, M. G. Brown, and R. J. Saykally, Science **284**, 945 (1999).
[24] G. C. Groenenboom, E. M. Mas, R. Bukowski, K. Szalewicz, P. E. S. Wormer, and A. van der Avoird, Phys. Rev. Lett. **84**, 4072 (2000).
[25] G. C. Groenenboom, P. E. S. Wormer, A. Van Der Avoird, E. M. Mas, R. Bukowski, and K. Szalewicz, J. Chem. Phys. **113**, 6702 (2000).
[26] E. M. Mas, K. Szalewicz, R. Bukowski, and B. Jeziorski, J. Chem. Phys. **107**, 4207 (1997).
[27] E. M. Mas, R. A. Bukowski, K. A. Szalewicz, G. C. Groenenboom, P. E. S. Wormer, and A. Van Der Avoird, J. Chem. Phys. **113**, 6687 (2000).
[28] T. R. Dyke, K. M. Mack, and J. S. Muenter, J. Chem. Phys. **66**, 498 (1977).
[29] G. T. Fraser, Int. Rev. Phys. Chem. **10**, 189 (1991).
[30] T. A. Hu and T. R. Dyke, J. Chem. Phys. **91**, 7348 (1989).
[31] R. D. Suenram, G. T. Fraser, and F. J. Lovas, J. Mol. Spectrosc. **138**, 440 (1989).
[32] E. Zwart, J. J. Termeulen, and W. L. Meerts, Chem. Phys. Lett. **173**, 115 (1990).
[33] E. Zwart, J. J. Termeulen, and W. L. Meerts, Chem. Phys. Lett. **166**, 500 (1990).
[34] E. Zwart, J. J. Termeulen, W. L. Meerts, and L. H. Coudert, J. Mol. Spectrosc. **147**, 27 (1991).
[35] E. N. Karyakin, G. T. Fraser, and R. D. Suenram, Mol. Phys. **78**, 1179 (1993).
[36] N. Pugliano and R. J. Saykally, J. Chem. Phys. **96**, 1832 (1992).
[37] N. Pugliano, J. D. Cruzan, J. G. Loeser, and R. J. Saykally, J. Chem. Phys. **98**, 6600 (1993).
[38] Z. S. Huang and R. E. Miller, J. Chem. Phys. **91**, 6613 (1989).
[39] J. B. Paul, R. A. Provencal, and R. J. Saykally, J. Phys. Chem. A **102**, 3279 (1998).
[40] H. J. C. Berendsen, J. P. M. Postma, W. F. van Gunsteren, and J. Hermans, *Intermolecular Forces* (D. Reidel, Dordrecht, Holland, 1981).
[41] D. N. Bernardo, Y. B. Ding, K. Kroghjespersen, and R. M. Levy, J. Phys. Chem. **98**, 4180 (1994).
[42] W. L. Jorgensen, J. Chandrasekhar, J. D. Madura, and R. W. Impey, J. Chem. Phys. **77**, 5073 (1983).
[43] A. Rahman and F. H. Stillinger, J. Chem. Phys. **55**, 3336 (1971).
[44] O. Matsuoka, E. Clementi, and M. Yoshimine, J. Chem. Phys. **64**, 1351 (1976).
[45] S. Kuwajima and A. Warshel, J. Phys. Chem. **94**, 460 (1990).
[46] R. J. Wheatley, Mol. Phys. **87**, 1083 (1996).
[47] P. O. Astrand, P. Linse, and G. Karlstrom, Chem. Phys. **191**, 195 (1995).
[48] C. Millot and A. J. Stone, Mol. Phys. **77**, 439 (1992).
[49] I. C. Hayes and A. J. Stone, Mol. Phys. **53**, 83 (1984).
[50] W. Rijks and P. E. S. Wormer, J. Chem. Phys. **90**, 6507 (1989).
[51] H. E. G. Casimir and D. Polder, Phys. Rev. **73**, 360 (1948).
[52] W. H. Press, *Numerical Recipes in C: The Art of Scientific Computing*, 2nd ed. (Cambridge University Press, Cambridge, 1992).
[53] J. A. Odutola and T. R. Dyke, J. Chem. Phys. **72**, 5062 (1980).
[54] L. A. Curtiss and J. A. Pople, J. Mol. Spectrosc. **55**, 1 (1975).
[55] S. S. Xantheas and T. H. Dunning, J. Chem. Phys. **99**, 8774 (1993).
[56] E. M. Mas and K. Szalewicz, J. Chem. Phys. **104**, 7606 (1996).
[57] J. K. Gregory and D. C. Clary, Chem. Phys. Lett. **228**, 547 (1994).
[58] L. A. Curtiss, D. J. Frurip, and M. Blander, J. Chem. Phys. **1**, 2703 (1979).
[59] S. S. Xantheas, J. Chem. Phys. **104**, 8821 (1996).
[60] D. Feller, J. Chem. Phys. **96**, 6104 (1992).
[61] A. J. Stone, A. Dullweber, P. L. A. Popelier, and D. J. Wales, 3.2 ed.

(University of Cambridge, Cambridge, 1995). To download Orient code, please see http://www-stone.ch.cam.ac.uk/
[62] G. S. Kell, G. E. McLaurin, and E. Whalley, Proc. R. Soc. London, Ser. A **425**, 49 (1989).
[63] B. J. Smith, D. J. Swanton, J. A. Pople, H. F. Schaefer III, and L. Radom, J. Chem. Phys. **92**, 1240 (1990).
[64] D. J. Wales, Advances in Molecular Vibrations and Collision Dynamics **3**, 365 (1998).
[65] D. J. Wales, *Theory of Atomic and Molecular Clusters* 2 (Springer, Heidleberg, 1998).
[66] C. J. Cerjan and W. H. Miller, J. Chem. Phys. **75**, 2800 (1981).
[67] C. Millot, J. C. Soetens, M. Costa, M. P. Hodges, and A. J. Stone, J. Phys. Chem. **102**, 754 (1998).
[68] K. Liu, J. G. Loeser, M. J. Elrod, B. C. Host, J. A. Rzepiela, N. Pugliano, and R. J. Saykally, J. Am. Chem. Soc. **116**, 3507 (1994).
[69] K. Liu, J. D. Cruzan, and R. J. Saykally, Science **271**, 929 (1996).
[70] K. Liu, M. G. Brown, M. R. Viant, J. D. Cruzan, and R. J. Saykally, Mol. Phys. **89**, 1373 (1996).
[71] J. K. Gregory and D. C. Clary, J. Phys. Chem. **100**, 18014 (1996).
[72] M. J. Elrod and R. J. Saykally, Chem. Rev. **94**, 1975 (1994).
[73] M. P. Hodges, A. J. Stone, and S. S. Xantheas, J. Phys. Chem. A **101**, 9163 (1997).
[74] K. Liu, M. G. Brown, and R. J. Saykally, J. Phys. Chem. A **101**, 8995 (1997).
[75] C. J. Burnham, L. Jichen, S. S. Xantheas, and M. Leslie, J. Chem. Phys. **110**, 4566 (1999).